


RESEARCH ARTICLE

Open Access



# The WORMESH-II flatworm-like mesh robot with 2-DOF double joints

Ganegoda V. C. Rasanga<sup>\*</sup> , Kengo Hiraishi, Ryuichi Hodoshima and Shinya Kotosaka

## Abstract

This paper deals with the development of a flatworm-like mesh robot WORMESH-II, which is the second prototype in the WORMESH series inspired from a flattened and soft-bodied flatworm. The pedal locomotion is the primary locomotor of the flatworm that is continuous gliding propulsion along the bottom of the body. The significance of WORMESH series is use of multiple pedal waves to generate the locomotion. The WORMESH-II is a modular robot having a revolute joint system to interconnect two modules. Further, it contains two module types: control module (CM) and joint module (JM). Depending on their arrangements, WORMESH-II can be arranged in different module formations. First, this paper presents the design of WORMESH-II in which double joints capable of three-dimensional motion are introduced. Then, two locomotion gaits for translational and spinning locomotion are described for WORMESH-II in isotropic module formation. Three synchronized parallel pedal waves and one pedal wave loop by the new double joint mechanism were respectively utilized to generate translational and spinning motions of WORMESH-II for IMF. The proposed locomotion gaits were investigated by dynamics simulation and the experiment using the prototype of WORMESH-II. We have successfully demonstrated basic translational and spinning locomotion of WORMESH-II with the velocity of 2.8 mm/s and the angular velocity of 0.0043 rad/s, respectively.

**Keywords** Flatworm, Bio-inspired robot, Double joint mechanism, Locomotion based on multiple pedal waves, Simulation and experiment

## Introduction

There are many animals in nature, such as worms and snakes, that do not have clear locomotive apparatus but are able to move and adapt to their environment using their rhythmic body motion. This locomotion style is known as limbless locomotion, and worms and snakes are the most common evidence for crawling and limbless motions. Researchers have been studying the locomotion mechanism, and biologically inspired robots that incorporate the principle of the locomotion have been studied for many years. Worm-like crawling has two primary locomotion styles: peristaltic crawling and two-anchor

crawling. Earth worms exhibit the peristaltic crawling limbless motion as they are moving through a small hollow space. Peristaltic locomotion-mimicked robot systems have successfully approached to inspect pipes in the harsh narrow environments [1–3]. Two-anchor crawling is evidenced by inchworms, which occupy body to generate a successful locomotion. A recently implemented inchworm-like robot system has used to check pipe systems by [4] and [5]. Snake robots are another well-known bio-inspired locomotory robot system. They have a linear and flexible body shape, which facilitates locomoting on uneven ground [6] and sand [7], in narrow channels and pipes [8], and even in water [9]. Additionally, this body shape assists to climb on tree branches [10] and fly between trees. Although most worm and snake-like robots are beneficial because of their particular body shape, this intrinsic narrow shape can occasionally restrict the usability range when considering tasks like

\*Correspondence:

Ganegoda V. C. Rasanga  
charakagvc@gmail.com  
Graduate School of Science and Engineering, Saitama University,  
338-8570 Saitama, Japan



© The Author(s) 2023. **Open Access** This article is licensed under a Creative Commons Attribution 4.0 International License, which permits use, sharing, adaptation, distribution and reproduction in any medium or format, as long as you give appropriate credit to the original author(s) and the source, provide a link to the Creative Commons licence, and indicate if changes were made. The images or other third party material in this article are included in the article's Creative Commons licence, unless indicated otherwise in a credit line to the material. If material is not included in the article's Creative Commons licence and your intended use is not permitted by statutory regulation or exceeds the permitted use, you will need to obtain permission directly from the copyright holder. To view a copy of this licence, visit <http://creativecommons.org/licenses/by/4.0/>.

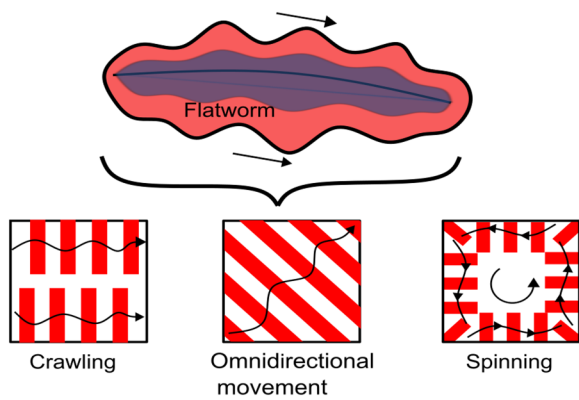


**Fig. 1** Concept of multiple travelling wave locomotion inspired by flatworms

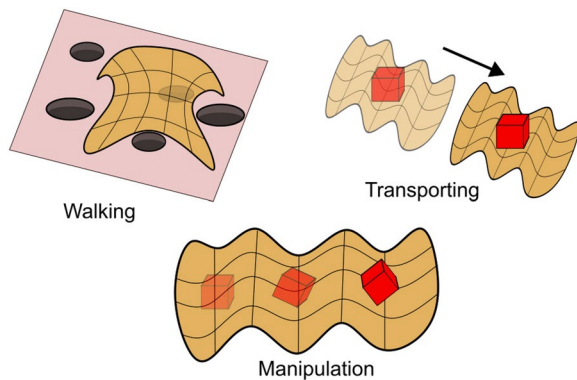


**Fig. 2** The function of the mesh structure in a sheet-like form

manipulation and carrying an object. These capabilities are advantageous for inspection and surveillance in an unstructured environment.

This study focuses on flatworms to embody flexibility and adaptability in robot technology that is different from snakes and worms that have been mechanized so far with the goal of creating a new form of limbless robot locomotion. We have been developing a mesh-like robot system called “WORMESH”, which is inspired by flatworms (Polycladida)[11]. They are dorsoventrally flattened, bilaterally symmetrical, and soft-bodied species, which can crawl on solid surfaces and swim in water. The key feature of flatworms is use of multiple travelling waves especially when swimming.

The concept of WORMESH is illustrated in Figs. 1 and 2. Flatworms use two body waves along their body; based on this feature, a flexible flat body can generate different locomotion by propagating travelling waves differently. This kind of two dimensional function body can move using independent travelling waves similar to the flatworm locomotion, and the flexible body allows

it to propagate waves in any direction. The ideal different crawling patterns are shown in Fig. 1, and red colour lines denote the relevant wave patterns. Additionally, this flexible functional body can walk on rough terrains while transporting and manipulating objects like Fig. 2. With respect to research on flattened cloth-like robots, for example, SheetBot [12] has been reported. In SheetBot, which aims to establish autonomous decentralized control, the theory of movement using travelling waves is not discussed, and the mechanical model developed is only a one-dimensional model similar to that of conventional snake-like robots. In addition, the flexible sheet-based Loco-Sheet [13] was developed to overcome discrete high terrain such as stairs, but its locomotion performance is limited due to the structure and number of Degree of Freedom (DOF).

In a previous study [14], the basic characteristics such as friction force and velocity related to pedal wave propulsion, which is the basic motion of WORMESH-II, were reported. On the other hand, this paper reports on the machine design theory and the development of an experimental machine for WORMESH-II, as well as the generation of multiple motions using Pedal wave, their characteristics, and experiments using mechanical models.

- Explain the design of double joint mechanism and hardware implantation of WORMESH-II.
- Develop travelling wave gaits for WORMESH-II using computer simulations. The introduced locomotion gaits are translational and spinning.
- Investigate the proposed locomotion gaits using the prototype of WORMESH-II.

### Concept of WORMESH-II: a flatworm-like robot with 2-DOF double joints

#### Overview

WORMESH-II is the second prototype that came with a new double-joint mechanism with better flexibility and degree of freedom than WORMESH-I. The primary design requirement of WORMESH is that the mesh-like functional body should generate multiple pedal waves along the robot body in any direction on the horizontal plane with maximum flexibility. For that, the modular concept was used to form the mesh structures by connecting modules via a revolute joints system which allows propagating travelling waves in any direction along the robot’s body. WORMESH-I was designed by connecting two consecutive cubic modules by a universal joint. That joint design created a larger gap between cubic modules by a cantilever type connecting elements of each cubic module, consequently caused the direct contact of joint

mechanism with the ground during locomotion and increased the required motor torque (Fig. 3a).

WORMESH-II has two types of modules, “Control Module (CM)” and “Joint Module (JM)” (Fig. 3b). Instead of the universal joint connection of WORMESH-I, JM allows locating a much better joint system with higher torque, flexibility, and reducing the distance between modules. CMs accommodate control hardware and power supply units, whereas JMs are utilized by motors, sensors, and linkages of the joint mechanism. Figure 4 shows the conceptual mechanical design of WORMESH-II. This module arrangement is named Isotropic Module Formation (IMF) because the number of modules is equal in each kinematic chain which interconnects nine CMs by twelve JMs according to mesh formation. Individual CMs are denoted by  $M_{ij}$  ( $i, j = 1, 2, 3$ ) and JMs by  $Mj_{ki}$  ( $k = x, y$  and  $i = 1, 2, \dots, 6$ ). Thus,  $M_{i1}-M_{i2}-M_{i3}$  ( $i = 1, 2, 3$ ) are the kinematic chains along the x direction, and  $M_{1i}-M_{2i}-M_{3i}$  ( $i = 1, 2, 3$ ) are the kinematics chains along the y direction. To generate the wave patterns like in Fig. 1, JM should provide the required DOF between two consecutive CMs.

**Joint mechanism design**

Figure 5a shows the conceptual design of mechanical connection between two consecutive CMs of WORMESH-II. Oppositely installed, two universal joints connect two consecutive CMs. Each universal joint has two revolute joints along pitch and yaw directions. The two universal joints are interconnected by a linkage mechanism, and this interconnected joint system is named as “2-DOF double-joint” system because joint angle between two

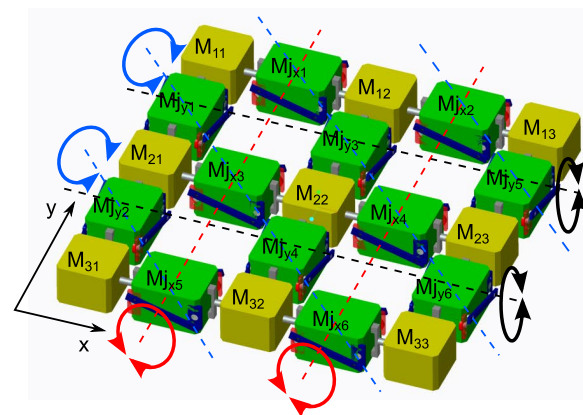


**Fig. 4** The basic design of WORMESH-II for the isotropic modules formation (IMF)

CMs is created by two set of universal joints in both pitch and yaw directions.

Figure 5b shows the conceptual mechanism design of the interconnected double-joint mechanism. Each pitch joint shaft ( $P_1$  and  $P_2$ ) has a simple mechanical bearing connection with two pitch links. One of the pitch links has a gear. Gear-pitch-link and pitch-link on the same side of  $P_1$  and  $P_2$  are interconnected by interconnecting-link. Spherical bearing joints,  $SB_1$  and  $SB_2$  interconnect yaw joint shaft  $Y_1$  and  $P_1$ ; similarly,  $Y_2$  and  $P_2$  are interconnected by  $SB_3$  and  $SB_4$ . Therefore, this mechanism can position shaft  $T_1$  and  $T_2$  in three-dimensional space, the output of the universal joints can control by the rotation of two gear pitch links. Figure 6 shows the pitch,

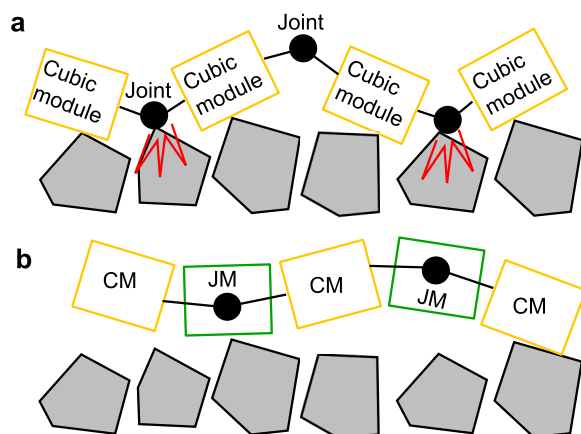


**Fig. 3** The difference between the WORMESH-I and WORMESH-II concepts. **a** WORMESH-I is composed of Cubic modules that are joined to one another via a joint mechanism. Because of this connection, the joint mechanism can make direct touch with the ground. **b** This issue was fixed in WORMESH-II by substituting a joint module for the joint mechanism that was used in WORMESH-I

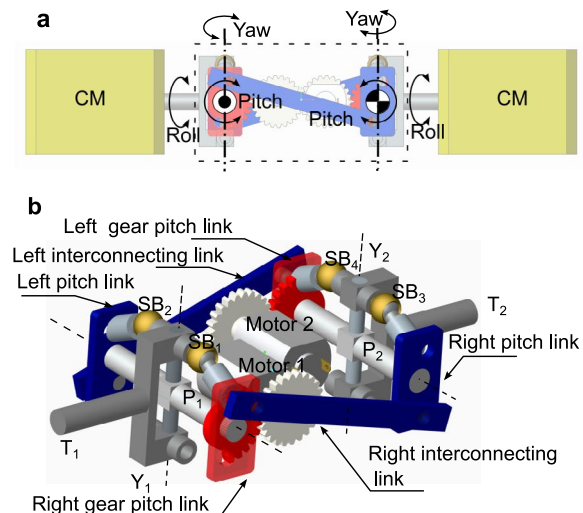


**Fig. 5** The idea behind WORMESH-II’s joint mechanism. **a** Connection between two CMs. **b** Conceptual design of active universal joint mechanism

yaw, and spinning movements of  $T_1$  and  $T_2$ , respectively. Motors,  $M_1$  and  $M_2$ , control the left and right gear pitch links. When a motor rotates one pitch link to a certain angle, the other pitch link on the same side of the next pitch axes rotates at the same time by almost the same angle by interlocking with the motion of the pair of links. Furthermore, two motors are individually controlled by an oscillation signal corresponding to each motor. The motion trajectory depends on the phase different ( $\Delta$ ) between  $M_1$  and  $M_2$  (Fig. 6). The trajectory of  $T_1$  and  $T_2$  moved in the 3D cartesian space, and trajectory of  $T_1$  is shown in Fig. 7. The trajectory of  $T_2$  is mirror image of  $T_1$ 's trajectory. Required conditions of two motors for pitch, yaw, circular spinning, and elliptical spinning motions are summarised as follows.

- Pitch motion: Same amplitude, same frequency and  $\Delta = 0$
- Yaw motion: Same amplitude, same frequency and  $\Delta = \pi$
- Circular spinning motion: Same amplitude, same frequency and  $\Delta = \pi/2$
- Elliptical spinning motion: Same amplitude, same frequency and  $0 < \Delta < \pi/2$

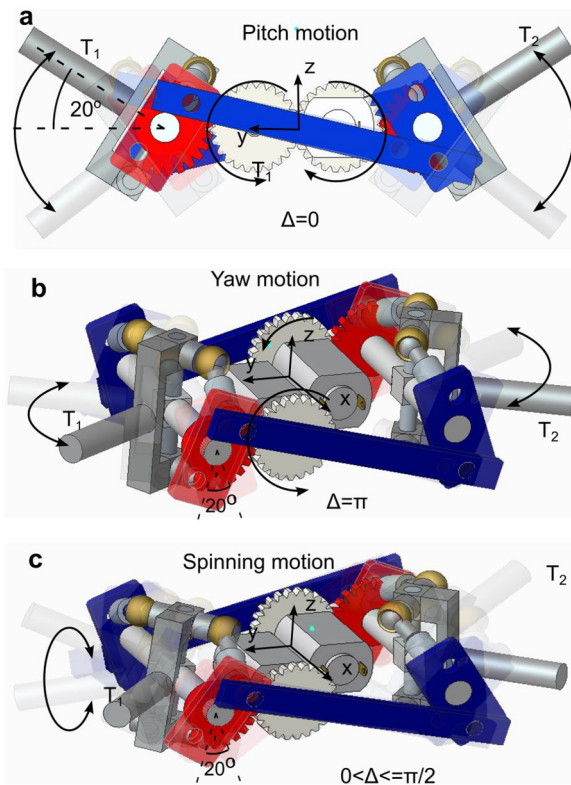


**Fig. 6** Kinematics of the active joint mechanism of WORMESH-II,  $\Delta$  is phase different between two motors. **a** Pitch. **b** Yaw. **c** Spinning

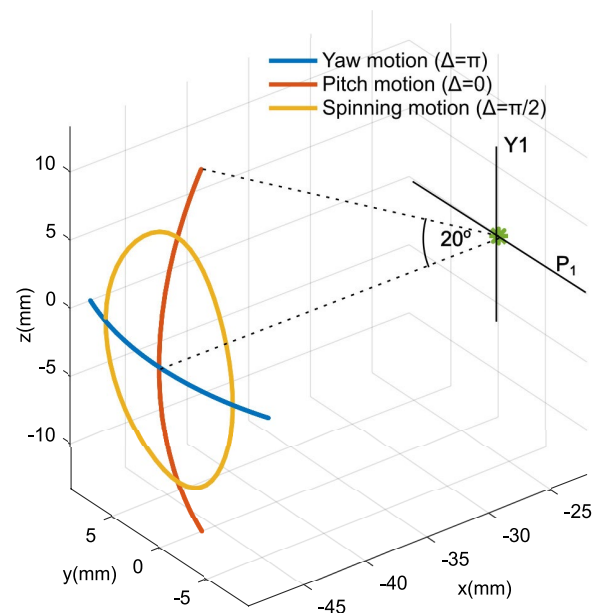


**Fig. 7** Workspace and trajectories of  $T_1$  corresponding to the coordinate frame in Fig. 6 for the joint angle ranging from  $0^\circ$  to  $\pm 20^\circ$  with respect to the centre of the  $P_1 - Y_1$  universal joint

### Prototype of WORMESH-II

#### Mechanical solution

Figure 8a shows the CAD designs of the implemented universal joint assembly corresponding to the concept of joint mechanism in Fig. 5. Another universal joint assembly was added to the system to improve flexibility between CMs. This universal joint has a revolute joint in roll ( $T_i$ ) and yaw ( $Yp_i$ ) directions, and joints are under spring loaded. Each  $T_i$  joint has four extension springs with spring constant of 0.78 N/mm, and each  $Yp_i$  has two extension springs (spring constant is 1.2 N/mm). The spring constant was determined by trial and error through experiment, and the joint mechanism has space to add more springs.

The mechanically implemented CAD design of a JM is illustrated in Fig. 8b. It comprises the gear mechanism, link mechanism, potentiometers and two micro metal geared DC motors. The bending angle of the interconnected active joints is measured by two potentiometers which are mechanically connected by DC motors with a super gear mechanism. The gear module of all gears is 0.5. The gear ratio between pitch-gear and motor-gear is 1:4.8. The gear ratio between motor-gear and gear of potentiometers is 1:1. Therefore, motor output shaft position is equal to the angular position of potentiometer. Moreover, vertical springs are connected with the top and bottom plates of the respective CM. Figure 8c shows the CAD design of a CM that has two power supply battery boxes, a microcontroller, and DC motor drivers. Each

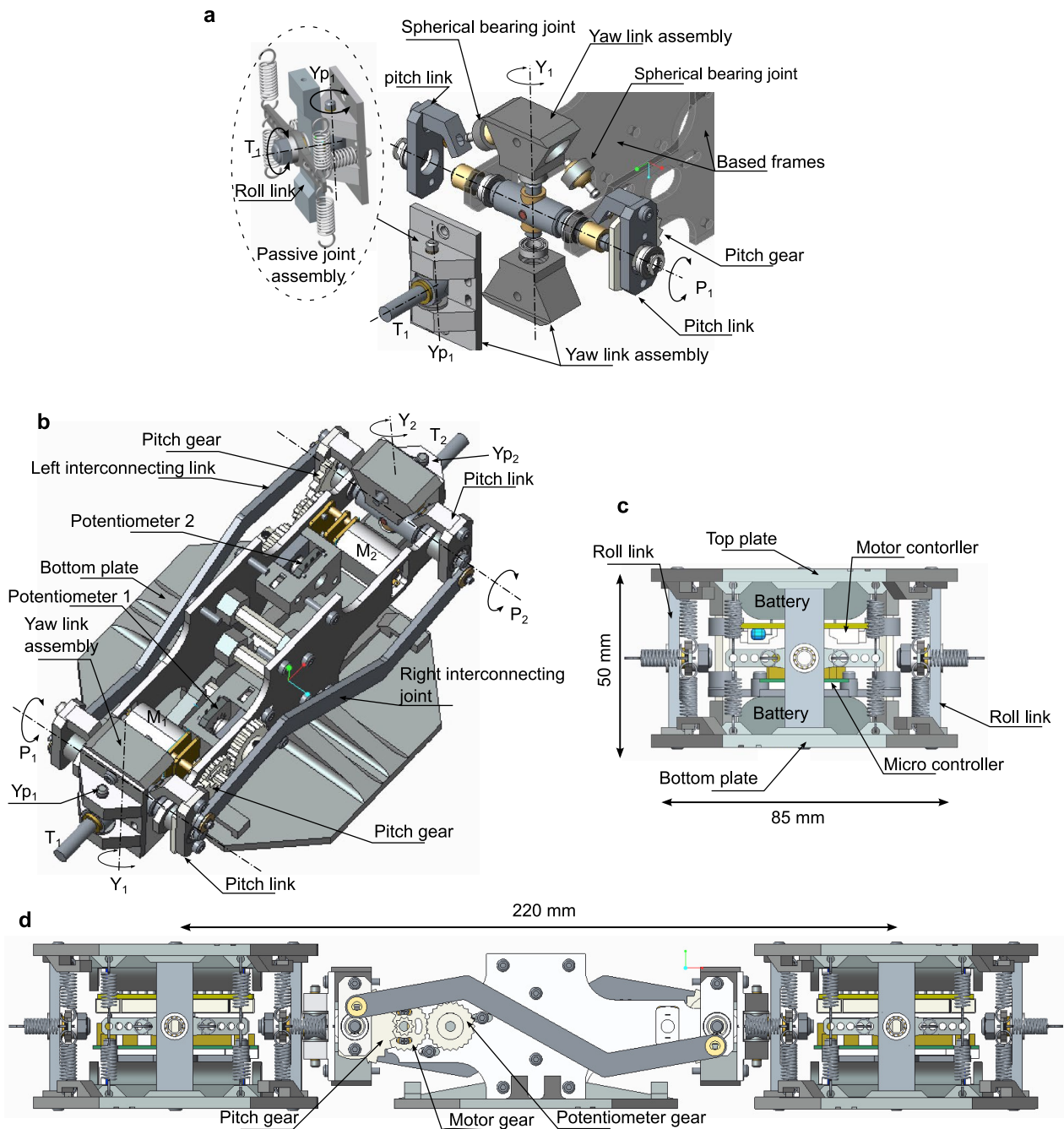


**Fig. 8** Mechanical design of joint mechanisms and modules. **a** Mechanical design of the universal joint assembly. **b** Mechanical design of JM. **c** Mechanical design of CM. **d** Complete mechanical design of connection between CM and JM

CMs can control either one or two joint mechanisms of the connected JMs. Figure 8d shows the implemented JM and its connection with CMs.

**System integration**

WORMESH-II is developed to be a self-contained robot system. Therefore, all power supply units,

microcontrollers and motor drivers are mounted on the CMs. Each CM has microcontroller unit, DC motor driver unit and power supply unit. Each power supply unit contains serially connected batteries supplying 12.3 V DC power. DC motor’s operation voltage range, the maximum output speed, torque at the maximum efficiency and stall torque are 6– 12 V, 100 rpm, 2 kg/

cm at 80 rpm, and 14 kg/cm, respectively. The micro-controller development board is “M3 HiBot TITech Tiny Controller,” a compacted, small controller board, which is one of the best solutions for compact robot designs. This control board has an STM32F205VCT7 core and sixteen analogues to digital conversion channels and many peripheral systems. The operating power range of M3 HiBot TITech Tiny controller is 5– 24 V. DC motors are controlled by BD6221 DC brush motor drivers.

Figure 9 displays the low-level control layout of WORMESH-II. The microcontroller program generates oscillation signals,  $\phi_{jik}$  ( $i = 1, 2, \dots, 6, j = x, y$  and  $k = 1, 2$ ), for each motor to control the joint position. The phase shift of the motor oscillation signal of a JM is denoted by  $\Delta_{jik}$ , and  $\Delta_{j11} - \Delta_{j12}$  controls the resulting motion type of joint either pitch, yaw or spinning (Figs. 6 and 7). The signal,  $\phi_{jik}$ , sends to the inbuilt PID controller to control DC motors. The actual joint position,  $\delta_{jik}$ , is calculated using potentiometers readings. Inbuilt PID controllers in the microcontrollers calculate the required PWM signals for BD6221 DC motor drivers. Each microcontroller in the CMs controls one or two JMs. CMs,  $M_{11}$ ,  $M_{22}$ , and  $M_{33}$  control two JMs. Each microcontrollers are interconnected by CAN bus. All oscillation signals are controlled according to the required locomotion gait. The CAN bus signals synchronise the oscillation signals of microcontrollers.

**Pedal wave locomotion of WORMESH-II**

The fundamental strategy of the pedal wave locomotion of WORMESH-II is to propagate synchronous parallel multiple pedal waves along the robot body to the

intended travelling direction [11]. The designed joint mechanism can create waves on the horizontal supporting plane in vertical and horizontal directions. However, the joint constraints between adjacent joints and modules restrict the curvature in the horizontal direction that parallel to the supporting plane. On the other hand, the joint mechanism of WORMESH-II can create a much better bending curvature on the vertical plane that is perpendicular to the supporting plane. The joint mechanism of WORMESH-II can generate pedal waves in any vertical plane perpendicular to the supporting plane (Fig. 1). Equation (1) expresses the joint angel ( $\phi$ ) between two consecutive links for the pedal wave locomotion, which controls the shape of the wave on 2D plane [15], where  $A$ , amplitude, is the maximum angle that can be achieved by  $\phi$ ; phase shift,  $\beta$ ;  $\omega$  is temporal wave frequency;  $i$  = joint number; and  $t$  = time.

$$\phi_{ti} = A \sin \{ \omega t + \beta(i - 1) \} (i = 1, 2, \dots, n) \quad (1)$$

**Modelling and control**

**Kinematics of multiple pedal wave locomotion**

Consider WORMESH-II on the horizontal plane at given time instant (Fig. 10). For translational motion, three synchronous parallel pedal waves were propagated along the three parallel kinematic chains [11], each kinematic chains has two grounding points ( $P_{i1}$  and  $P_{i2}$ ) at each time instant, and velocities are denoted by  $v_{i1}$  and  $v_{i2}$  at  $P_{i1}$  and  $P_{i2}$  ( $i=1,2,3$ ), respectively. The coordinate of COG (Center of geometry) on  $X_g Y_g$  global frame is  $(X, Y)$ . The local frame on the COG of the robot is denoted by  $xy$ . Assumed each

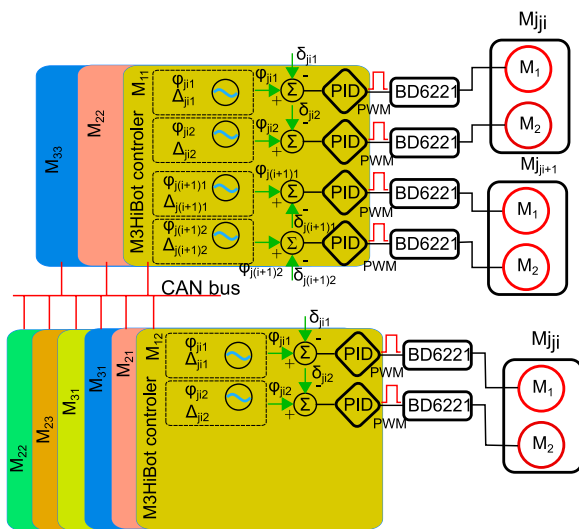


Fig. 9 Control system layout of WORMESH-II

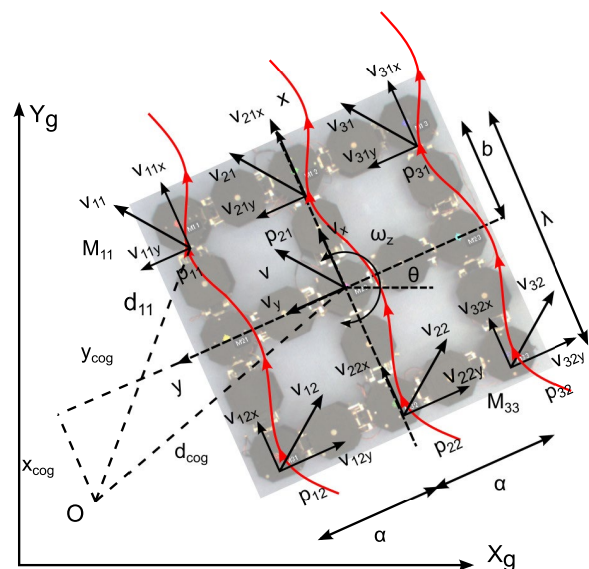


Fig. 10 Locomotion kinematics model of WORMESH-II

kinematic chains generates two wave shapes. Thus, distance between  $P_{i1}$  and  $P_{i2}$  is  $\lambda$ , and between  $P_{ij}$  and  $P_{(i+1)j}$  ( $i=1,2,3$  and  $j=1,2$ ) is  $a$ . Assumed COG has linear velocity vector,  $v = [v_x, v_y, 0]$  and angular velocity vector,  $\omega_z = [0, 0, \omega_z]$ . State vector  $q$  of WORMESH-II with respect to  $X_g Y_g$  can be defined as  $q = [X, Y, \theta]^T$ . Hence, generalised velocity vector  $\dot{q}$  can be represented by  $\dot{q} = [\dot{X}, \dot{Y}, \dot{\theta}]^T$ . Thereby,

$$\begin{bmatrix} \dot{X} \\ \dot{Y} \\ \dot{\theta} \end{bmatrix} = \begin{bmatrix} \cos\theta & -\sin\theta & 0 \\ \sin\theta & \cos\theta & 0 \\ 0 & 0 & 1 \end{bmatrix} \begin{bmatrix} v_x \\ v_y \\ \omega_z \end{bmatrix} \quad (2)$$

The velocity of each kinematic chain depends on its pedal wave parameters,  $A, \omega$  and  $\beta$  (Eq. 1). Considering overall linear displacement along the wave propagation direction of a kinematic chain, for a unit locomotion cycle, the average velocities  $v_{i1x}$  and  $v_{i2x}$  in the wave propagation direction at  $P_{i1}$  and  $P_{i2}$  should be equal and are denoted by  $v_{ix}$ . Hence,  $v_{i1x}$ ,  $v_{i2x}$  and  $v_{ix}$  ( $i = 1, 2, 3$ ) can be expressed as a function of pedal wave parameters (Eq. 3).

$$v_{ix} = v_{i1x} = v_{i2x} = f(A_i, \omega_i, \beta_i) \quad (i = 1, 2, 3) \quad (3)$$

Function  $f$  denotes the relationship between average linear velocity and travelling wave parameters. If there are no slips at ground contact points, the relationship between  $\omega$  and  $v_{ix}$  is proportional and linear. The relationship between  $A$  and  $v_{ix}$  is proportional, and  $\beta$  controls the moving direction [16].

$$\begin{aligned} \omega_z &= \frac{v_{11x}}{y_{COG} - a} = \frac{v_{21x}}{y_{COG}} = \frac{v_{31x}}{y_{COG} + a} = \frac{v_x}{y_{COG}} \\ &= \frac{v_{y1}}{x_{COG} + b} = \frac{v_{y2}}{\lambda - b - x_{COG}} = \frac{v_y}{x_{COG}} \end{aligned} \quad (4)$$

Considering rotation around an instantaneous centre of rotation  $O$ , Eq.(4) was derived. There is no relative motion between CM in the kinematic chain along the lateral direction to the wave propagation direction. Hence,  $v_{i1y} = v_{y1}$  and  $v_{i2y} = v_{y2}$  ( $i = 1, 2, 3$ ), and all average velocity component at each grounding point can be expressed as follow for a unit locomotion cycle.

$$\begin{bmatrix} v_{1x} \\ v_{2x} \\ v_{3x} \\ v_{y1} \\ v_{y2} \end{bmatrix} = \begin{bmatrix} 1 & -a \\ 1 & 0 \\ 1 & a \\ 0 & x_{COG} + b \\ 0 & \lambda - b - x_{COG} \end{bmatrix} \begin{bmatrix} v_x \\ \omega_z \end{bmatrix} \quad (5)$$

Using Eq.(3), Eqs.(4) and (5),  $v_x$  and  $\omega$  can be defined as follow.

$$\begin{bmatrix} v_x \\ \omega_z \end{bmatrix} = \begin{bmatrix} \frac{f(A_1, \omega_1, \beta_1) + f(A_2, \omega_2, \beta_2) + f(A_3, \omega_3, \beta_3)}{3} \\ \frac{f(A_1, \omega_1, \beta_1) - f(A_3, \omega_3, \beta_3)}{2a} \end{bmatrix} \quad (6)$$

Considering Fig. 10 and Eq.(6), locomotion kinematics of WORMESH-II can be described as follows. The overall translational displacement is resulted from the individual contribution of each active kinematic chain. Hence, the average translational velocity of COG ( $v_x$ ) is a function of the travelling wave parameter of individual kinematic chain (Eq. 3). By considering linear motion of individual kinematic chains,  $v_x$  can be approximated to average of  $v_{1x}$ ,  $v_{2x}$ , and  $v_{3x}$ . Moreover, the angular velocity,  $\omega_z$ , is proportional to the average velocity difference of kinematic chains, one and three. When kinematic chain one and three have equal wave parameters, ideally robot moves in a straight line.

When considering wave amplitude,  $A$ , and phase shift,  $\beta$ , the relationship between linear velocity and pedal wave parameters is a non-linear function. Physics-engine based dynamic simulation provides much more accurate results in robot locomotion. Therefore, to validate the mathematical explanation of multiple pedal wave locomotion, locomotion of WORMESH-II was simulated using dynamics simulations of CoppeliaSim.

### Simulation setup

The simulation robot model was generated resembling WORMESH-II by connecting rectangular-shaped cubes with revolute joints according to the mesh formation. Figure 11 shows the kinematic models of the joint mechanism of IMF in the simulation environment. CMs and JMs are denoted by yellow and green squares, respectively. Pitch joints of each kinematics chain in the longitudinal and transverse directions are denoted by  $PX_{ik}$  and

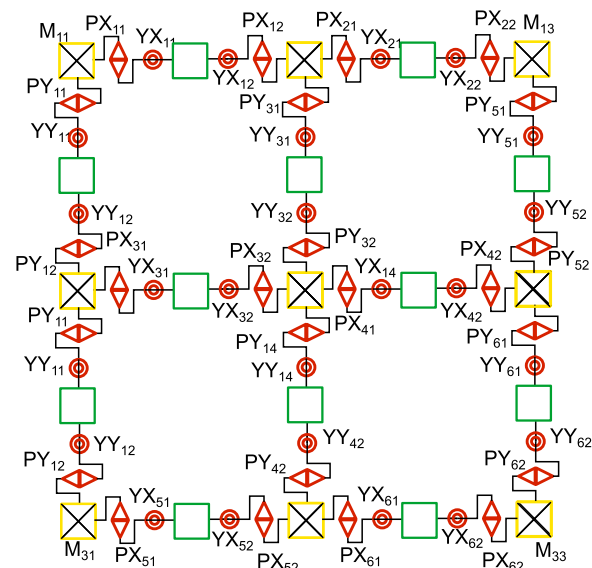


Fig. 11 Joint kinematic models of the simulation model of WORMESH-II

$PY_{ik}$  ( $k = 1, 2; i = 1, 2, \dots, 6$ ), respectively. Likewise, Yaw joints are denoted by  $YX_{ik}$  and  $YY_{ik}$  ( $k = 1, 2; i = 1, 2, \dots, 6$ ). Passive joints were not illustrated in this diagram for the simplicity and contraction of the figure size. Pure geometric shapes were only used to increase the accuracy of dynamic simulation. The interconnected link mechanism was not included in the simulation model, and each active pitch and yaw joint is individually controlled in the simulation program according to the required locomotion gait.

## Simulation

### Translational motion

As Fig. 10, three synchronous pedal waves were propagated along the kinematic chains with equal  $A, \omega$  and  $\beta$  to move the robot in translational direction (Eq. 6). Each revolute pitch joints of each kinematic chains was controlled according to Eq. (1). Relative bending angle between two consecutive CMs is equal to  $\phi_{ti}$ . To generate the translational locomotion of WORMESH-II for IMF in the  $X$  direction, three pedal waves were used along the kinematic chains,  $M_{11} - M_{12} - M_{13}$ ,  $M_{21} - M_{22} - M_{23}$  and  $M_{31} - M_{32} - M_{33}$  (Fig. 4). Similarly to generate the translational locomotion in  $Y$  direction, three pedal waves were used along the kinematic chains,  $M_{11} - M_{21} - M_{31}$ ,  $M_{12} - M_{22} - M_{32}$  and  $M_{13} - M_{23} - M_{33}$  (Fig. 4).

The movements of robot in the simulation environment is shown in Fig. 12. As discussed in [14], translational locomotion of IMF is not continuous but a sequence of four locomotion steps. Figure 12 reveals the corresponding robot poses of those locomotion steps during one locomotion cycle ( $t = 0.6$  s, 1.11 s, 1.6 s, and 2 s).

Link poses and their velocities towards the travelling direction at the ground contact points  $P_i$  ( $i = 1, 2, \dots, 10$ ) of robot are illustrated in Fig. 13. All three kinematic chains, which propagate three pedal waves synchronously, have the same pedal wave parameters. These link poses further realized that the pedal wave locomotion of robot for IMF is not a continuous locomotion wave, because there are only three links per one kinematic chain, which is the minimal requirement to generate the travelling wave in a series kinematic chain. To generate a stable continuous pedal wave on the horizontal plane, each kinematic chains should capable to form at least two wave shapes along the kinematic chain. Moreover, when CMs per one kinematic chain is equal to three, it is impossible to generate two complete pedal wave shapes.

The translational locomotion gait of robot is like an inchworm locomotion based on the anchor crawling motion principle [17]. According to links poses and movement of ground contacted points, robot motion can be understood clearly using anchor crawling motion principle. In Fig. 13b, for simulation time ( $t$ ) from 0 to

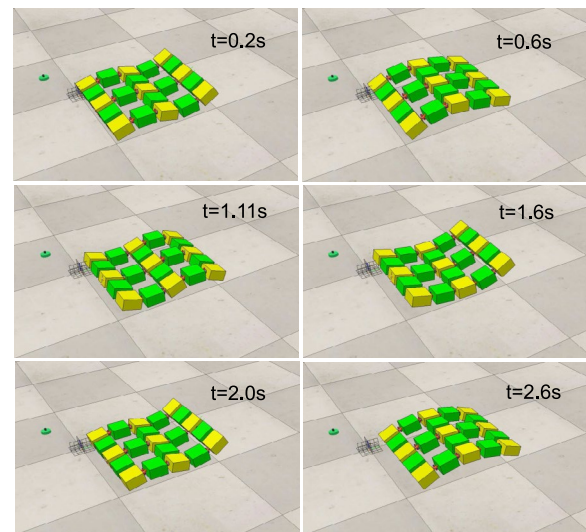


**Fig. 12** Translational locomotion of WORMESH-II for IMF in the simulation (wave parameters are  $A = 0.05\pi$ ,  $\omega = 0.5\pi$ , and  $\beta = 4\pi/3$ )

0.3 s, the ground contact point at the rear side ( $P_{10}$ ) of kinematic chain has positive velocity towards the travelling direction (0.025 m/s), whereas the ground contact point at the front area ( $P_2$  and  $P_3$ ) has almost zero velocity. Like the anchor-pull of inchworm locomotion discussed in [17], during this locomotion step, the front area of robot anchors the ground while rear side pulls towards. From simulation time 0.9 to 1.2 s, both front  $P_1$  and rear ends  $P_{10}$  contact the ground and approximately do not move towards the travelling direction (Fig. 13c). At the next stage,  $t = 2.1 - 2.4$  s, WORMESH-II's front end  $P_1$  skid towards the travelling direction whilst the  $P_6$  and  $P_7$  of kinematic chains anchors the ground. This motion is pair with the Anchor-push of inchworm locomotion (Fig. 13d). During  $t = 2.7 - 3.0$  s, link poses transfer from anchor-pull motion to anchor-push motion (Fig. 13e). The average locomotion speed of the Centre of Geometry (COG) towards the travelling direction of robot was 11.4 mm/s.

### Spinning motion

Kinematics of spinning around the COG can be qualitatively explained by Eq.(6). Angular velocity  $\omega_z$  is proportional to the velocity difference of kinematic chains, one and three (Fig. 10). Thus, according to mathematical explanation, when the wave propagation direction of both waves are opposite to each other and kinematic chain two is neutral,  $v_x = 0$ , and the robot is spinning around COG. It can be called differential wave formation. Furthermore, the square shape module formation of WORMESH-II can generate differential wave formation in longitudinal



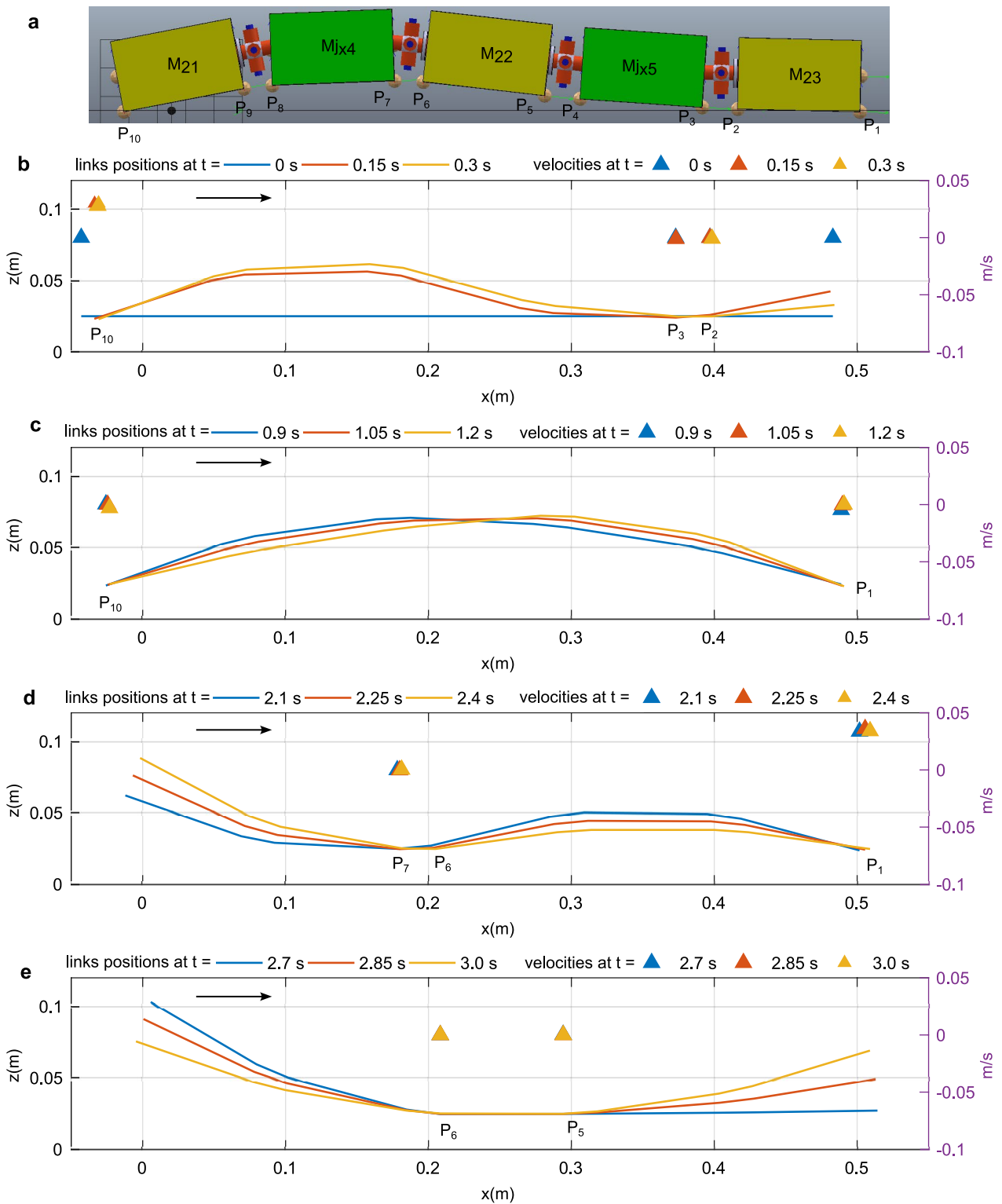


**Fig. 13** In translational locomotion simulation, the link locations and velocities at the ground contact points of WORMESH-II with respect to time  $t$  (wave parameters are  $A = 0.05\pi$ ,  $\omega = 0.5\pi$ , and  $\beta = 4\pi/3$ ). **a** Terminology of ground contact points. **b** Anchor-pull movement. **c** From Anchor-pull to Anchor-push. **d** Anchor-push movement **e** From Anchor-push to Anchor-pull

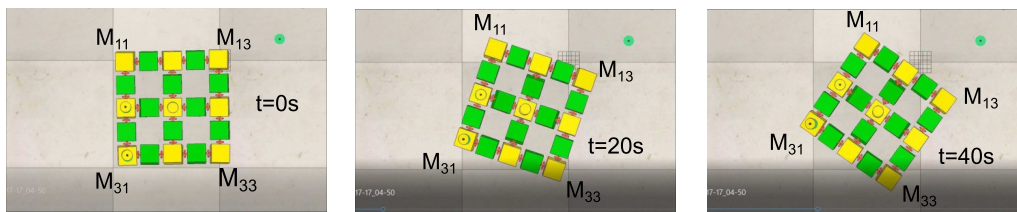


**Fig. 14** Spinning locomotion of WORMESH-II for IMF in simulation (wave parameters are  $A = 0.05\pi$ ,  $\omega = \pi$ , and  $\beta = 4\pi/3$ )

and transverse directions like the spinning concept in Fig. 1 using four kinematic chains. The sequence of kinematics chains are  $M_{11} - M_{12} - M_{13}$ ,  $M_{13} - M_{23} - M_{33}$ ,  $M_{33} - M_{32} - M_{31}$ , and  $M_{31} - M_{21} - M_{11}$ .

The spinning direction depends on the direction of wave propagation, which is controlled by changing  $\beta$

in Eq. (1). Figure 14 shows the locomotion poses of the simulation model of the robot during spinning. The simulated robot poses confirmed that the proposed pedal wave gait can successfully change the orientation around the COG of WORMESH-II. The corresponding pedal wave parameters were  $A = 0.05\pi$ ,  $\omega = \pi$ , and

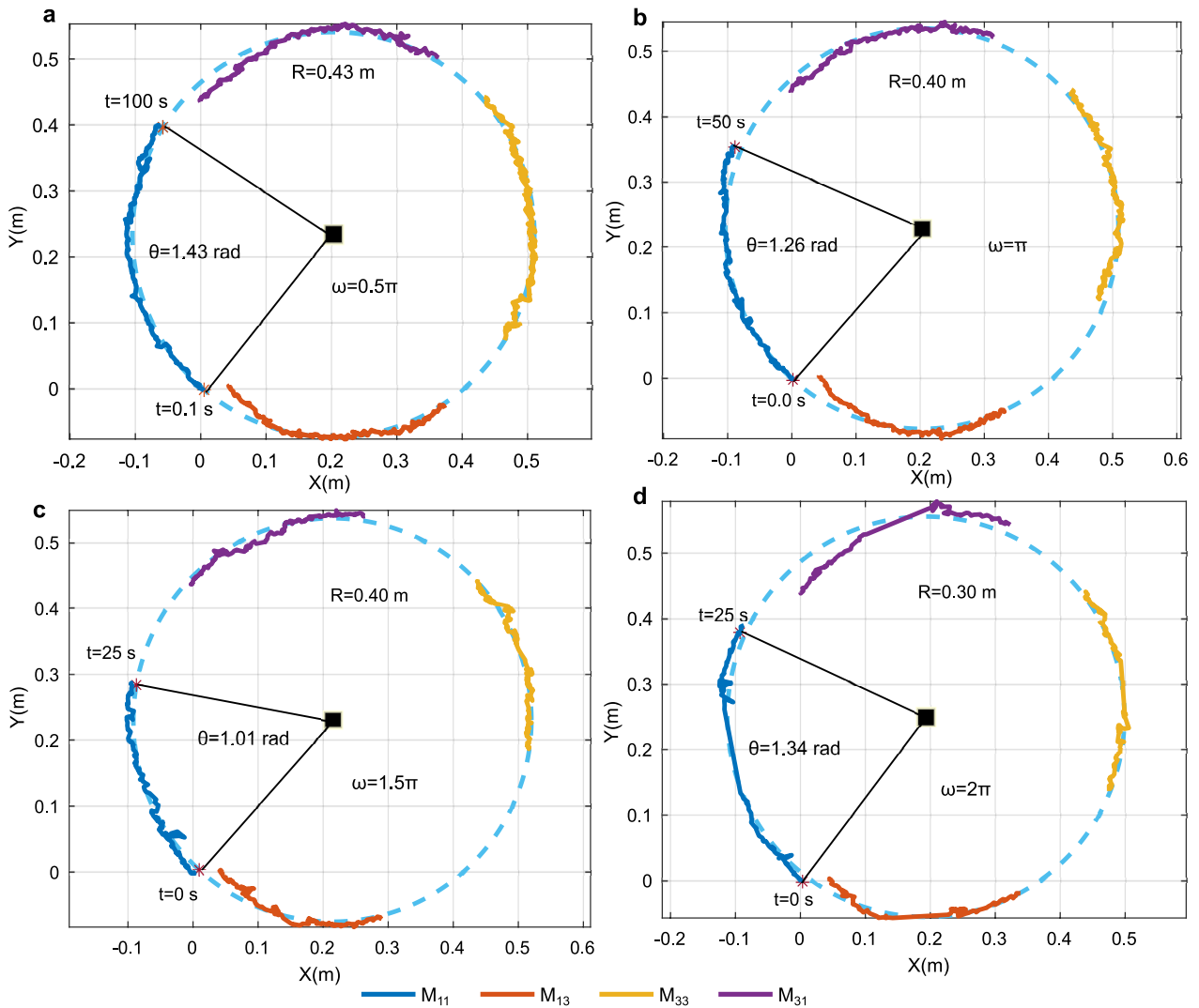


**Fig. 15** Simulated trajectories of CMs  $M_{11}$ ,  $M_{13}$ ,  $M_{33}$ , and  $M_{31}$ , for spinning locomotion of WORMESH-II for IMF (wave parameters are  $A = 0.05\pi$  and  $\beta = 4\pi/3$ ). **a**  $\omega = \pi/2$ . **b**  $\omega = \pi$ . **c**  $\omega = 3\pi/2$ . **d**  $\omega = 2\pi$

$\beta = 4\pi/3$ . The trajectories of CMs,  $M_{11}, M_{13}, M_{33}$ , and  $M_{31}$ , on the  $XY$  plane (horizontal plane) are shown in Fig. 15 for different  $\omega$  values. These trajectories depict a smooth and perfect spinning motion around the COG of WORMESH-II. Also, the average angular velocity around the COG of WORMESH-II increased with  $\omega$  of the pedal wave, but at low  $\omega$ , the robot trajectory was much controllable and smoother than the higher  $\omega$ .

## Experiment with prototype

### Translational motion

Translational locomotion of WORMESH-II's prototype was tested for the IMF based on the simulation. The pedal wave parameters were  $A = 0.13\pi$ ,  $\omega = \pi/20$ , and  $\beta = 1.5\pi$ . Three parallel synchronous pedal waves were used to generate the translational motion of prototype as same as the simulation. Every four motors in each kinematic chain generated the required joint angle according to the oscillation signal sent from the connected microcontroller. Figure 16 shows the locomotion poses of WORMESH-II's prototype for IMF. Like in the simulation, prototype also creates the translation locomotion based on the sequence of anchor-push and anchor-pull locomotion steps. From  $t=0.67$  s to 2.67 s is anchor-pull locomotion step,  $t = 5.33 - 6.67$  s is anchor-push locomotion step (Fig. 16). The relevant video is included in Additional file 1. The trajectory of  $M_{22}$  is shown in Fig. 17. Total disparagement in wave propagation direction is 500 mm. However, there was a -40 mm and 25 mm side displacement in the lateral direction to the wave propagation direction. Robot movement from the top is shown in Fig. 21 (video is included in Additional File 3) in Appendix. The average locomotion speed is 2.8 mm/s.

### Spinning locomotion

The spinning locomotion of the robot is shown in Fig. 18 and relevant video is included in Additional file 2. The proposed differential pedal wave loop created a successful spinning motion around the COG of WORMESH-II. The wave loop was propagated along kinematic chain,  $M_{11} - M_{12} - M_{13}$ ,  $M_{13} - M_{23} - M_{33}$ ,  $M_{33} - M_{32} - M_{31}$ , and  $M_{31} - M_{21} - M_{11}$ . The turning direction relies on the wave propagation direction. The average angular velocity around the COG is 0.0043 rad/s for  $A = 0.12\pi$ ,  $\omega = \pi/20$  and  $\beta = 1.5\pi$ . Figure 19 shows trajectories of CMs,  $M_{11}, M_{13}, M_{33}$  and  $M_{31}$ . The turning circle radius of 310 mm is approximately equal to the diagonal length of the robot.

## Discussion

Locomotion using multiple travelling waves is a hardly discussed topic, and this feature provides more flexible and adaptable locomotion capability in different

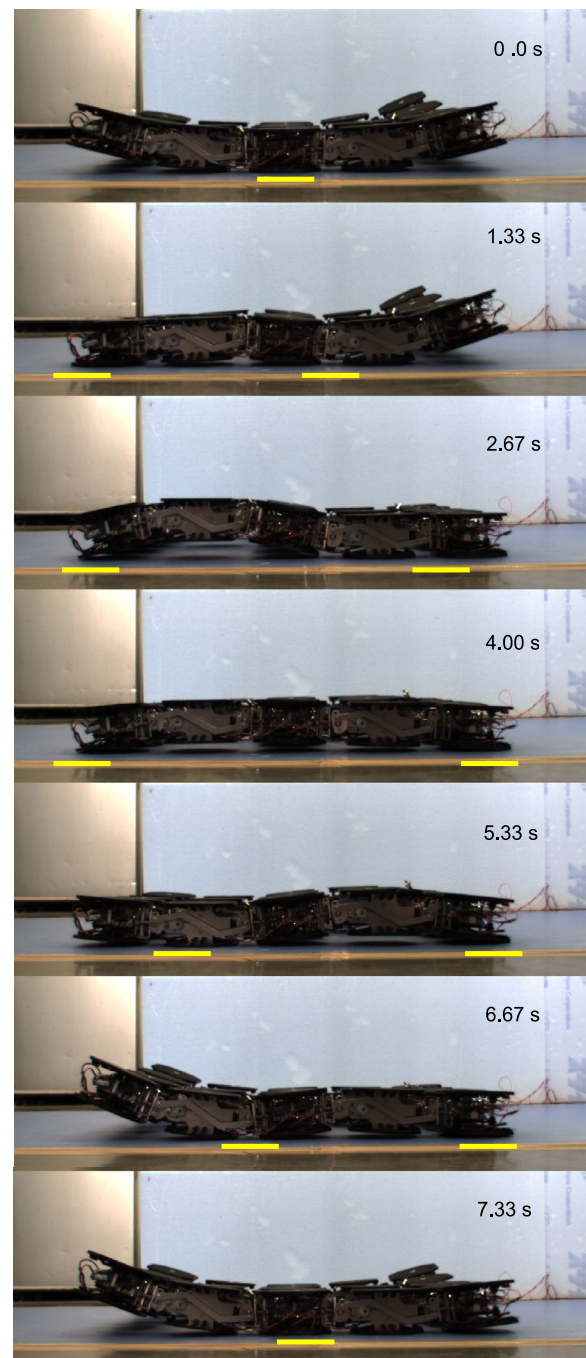


**Fig. 16** Translational locomotion of WORMESH-II for IMF (wave parameters are  $A = 0.13\pi$ ,  $\omega = \pi/20$ , and  $\beta = 3\pi/2$ )

terrain conditions. Combinations of different travelling waves can allow WORMESH-II to move differently. The performance of this kind of mesh-like function body mainly depends on the joint mechanism and its flexibility. A compacted flexible joint system with higher DOF is an advantage. Figure 20 shows the overall size of both

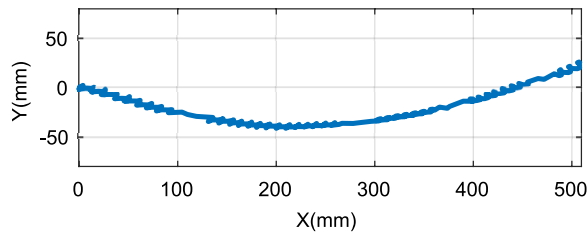


**Fig. 17** Trajectory of  $M_{22}$  (COG) of translational locomotion (wave parameters are  $A = 0.13\pi$ ,  $\omega = \pi/20$ , and  $\beta = 3\pi/2$ )

prototypes of WORMESH-I and WORMESH-II. The width and length of WORMESH-II are 94 mm larger than WORMESH-I. However, WORMESH-II has 21 cubic modules. The joint module concept reduced the centre-to-centre distance between consecutive cubic modules from 170 mm to 110 mm. That reduced the gap between consecutive cubic modules from 86 mm to 23 mm. It is the main advantage to move on an uneven surface (Fig. 3). The proposed double-joint mechanism controls the motion of consecutive CMs using two interconnected universal joints. Only two DC motors need to control two interconnected universal joints, reducing the

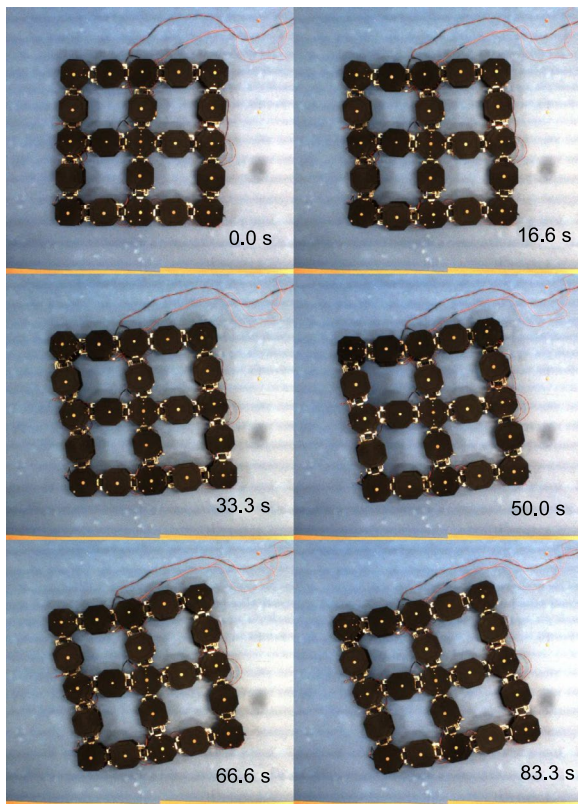


**Fig. 18** Spinning locomotion of WORMESH-II (wave parameters are  $A = 0.12\pi$ ,  $\omega = \pi/20$ , and  $\beta = 3\pi/2$ )

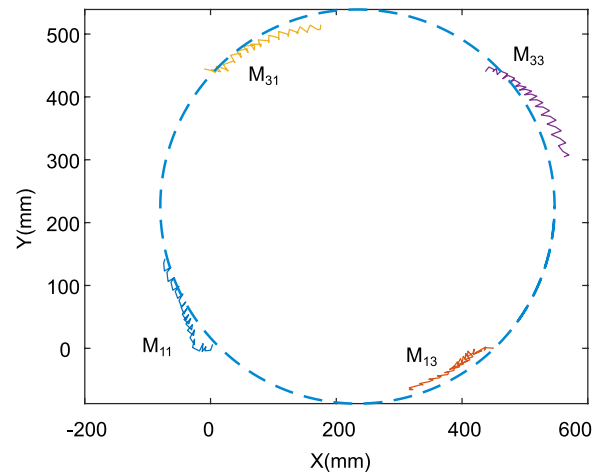


**Fig. 19** Trajectory of  $M_{11}$ ,  $M_{13}$ ,  $M_{33}$  and  $M_{31}$  of spinning locomotion of WORMESH-II (wave parameters are  $A = 0.12\pi$ ,  $\omega = \pi/20$ , and  $\beta = 3\pi/2$ )

size and weight of JMs. The spring-loaded passive joints system reduced the joint constraint from nearby CMs and improved the mesh structure’s flexibility. However, at the higher omega, sometime connection between pitch

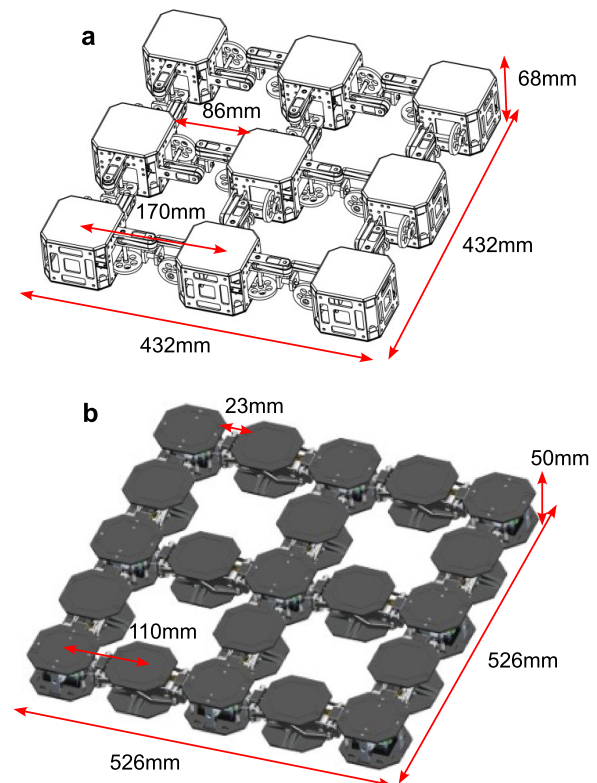


**Fig. 20** Complete design of both prototypes. **a** WORMESH-I. **b** WORMESH-II

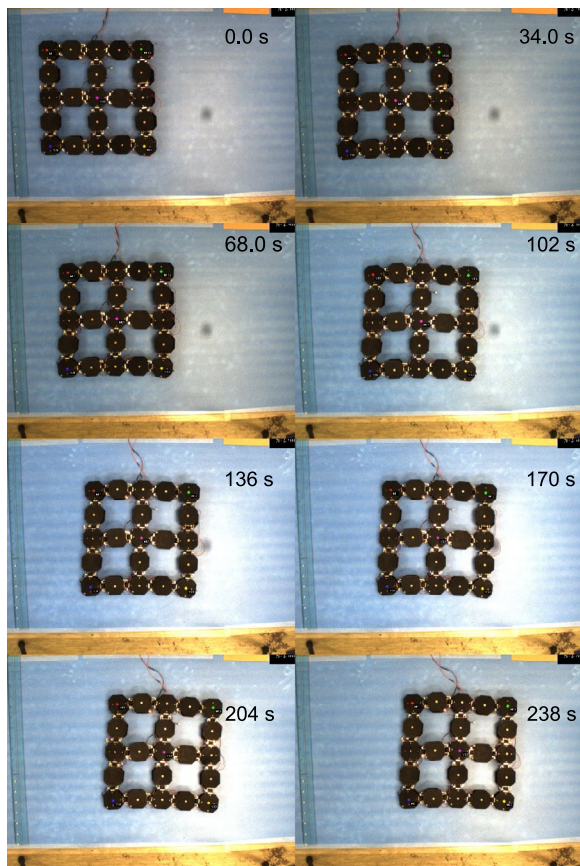


**Fig. 21** Translational locomotion of WORMESH-II for IMF (wave parameters are  $A = 0.13\pi$ ,  $\omega = \pi/20$ , and  $\beta = 3\pi/2$ )

gear and motor gear failed by misalignment, and this should be improved.

The mathematical explanation of multiple pedal wave locomotion proved that the locomotion of robot is dependent on the average linear velocity of individual kinematic chains and wave propagation directions. These velocity components rely on wave amplitude and temporal frequency. However, unequal temporal frequencies would limit the curvature of the adjacent kinematic chains because of mesh formation. Therefore, all travelling waves were synchronized. Thereby, wave amplitude is the control parameter. The horizontal moving distance,  $\Delta x$ , for one period of a pedal wave is equal to  $L - \lambda$ ,  $\lambda$  is the wavelength,  $L$  is the length of the arc of one wave which is equal to  $L_T/k$  ( $L_T$ : total length of the kinematic chain, and  $k$  is the number of complete wave shapes). For the above relation,  $k \geq 2$  and there are no relative motions at the grounding points. The wave amplitude depends on  $\lambda$ , since  $L_T$  is constant, and higher amplitude means a lower  $\lambda$ . However, the relationship between the average velocity of individual kinematic chains and wave

amplitude is challenging to explain quantitatively because the relationship between wave amplitude and  $\lambda$  is not linear, when  $k < 2$  for the simulation and experiment setup of WORMESH-II. Nonetheless, mathematical model of multiple pedal wave locomotion explains the locomotion of WORMESH-II qualitatively (Eq. 6). The result of simulations and experiments confirmed the qualitative explanation of the multiple pedal wave locomotion of WORMESH-II according to the locomotion kinematic model (Additional file 1).

In accordance with the discrete locomotion behaviour of WORMESH-II, [14] developed an adaptive locomotion gait by modulating amplitude throughout the kinematic chains in order to traverse frictional transition circumstances. Nevertheless, detecting frictional conditions is a difficult task. This work defined translational movement based on inchworm crawling, making it easy to comprehend the three-link pedal wave locomotion. The overall locomotion can be enhanced by applying simple high-friction materials to the bottom plate of JMs (Fig. 13a). However, it needs to be concerned about the JMs of the kinematic chain in the lateral direction to the wave propagation direction. This method is possible for JMs  $M_{j_{x3}}$ ,  $M_{j_{x4}}$ ,  $M_{j_{y3}}$ , and  $M_{j_{y4}}$  (Fig. 4).

There was some lateral movement in the trajectory of the translational motion (Fig. 17). The side-slipping was caused by the passive joint system. If the yaw joints ( $Y_{p_i}$ ) aren't very rigid, the direction of motion will shift. According to the simulation when joints with a spring constant above 4 Nmm trajectories were controllable. By making the springs of passive joints tighter, side-slipping movement can be reduced. But because passive joints were stiffer, they needed more torque from the motor and made the mesh structure less flexible. Optimised spring mechanism of passive joint will be discussed in the future.

In spinning motions, the centre of the robot always makes contact with the ground. That would increase the surface friction and decrease the turning speed. If a pyramid-like pose is created with JMs ( $M_{j_{x3}}$ ,  $M_{j_{x4}}$ ,  $M_{j_{y3}}$ , and  $M_{j_{y4}}$ ) in the middle, the turning speed can be enhanced.

## Conclusion

Introducing a newly suggested unique robot called WORMESH-II with a 2-DOF double joint mechanism was the key aspect of this study. The concept of WORMESH-II was developed, inspired by the locomotion of flatworms. Flatworms use two pedal waves along the body when swimming (Fig. 1). Multiple pedal waves were utilized to generate the locomotion of this robot. The combination of different travelling waves allows

the robot to move in different ways, which would be an advantage of locomotion in different terrain conditions. In addition, mesh-like functional body has potential to walk, transport and manipulate (Fig. 2) (Additional file 3).

The introduced joint mechanism controls two universal joints by two DC motors. In WORMESH-I, each universal joint needed two motors to control its revolute joint in pitch and yaw axis. The 2-DOF double joint mechanism reduced the required number of motors, and spring-loaded passive joints improved the flexibility of the structure. Overall, the double joint mechanism is compact and has a higher DOF (Fig. 6 and 8).

The mathematical modelling of locomotion kinematics, simulations and experiments of WORMESH-II evidenced that the proposed multiple pedal wave locomotion methods can successfully generate translational and spinning locomotion. In simulation for  $\omega = 0.5\pi$   $\text{rads}^{-1}$ , the average linear velocity of translation locomotion ( $v_x$ ) was  $11.4 \text{ mms}^{-1}$ , and the average average velocity of spinning ( $\omega_z$ ) was  $0.025 \text{ rads}^{-1}$ . When experimenting with the real robot,  $\omega$  was kept at a low value ( $\pi/20 \text{ rads}^{-1}$ ) to eliminate gear teeth shifting. that is the reason for low  $v_x$  and  $\omega_z$ . For experiment with real robot,  $v_x = 2.8 \text{ mms}^{-1}$  and  $\omega_z = 0.0043 \text{ rads}^{-1}$ .

In future works, it needs to develop a control system to move WORMESH-II by combining translational and spinning motions. The control system is recommended to be further advanced by shifting capability to translational gait and spinning gait for a locomotion with smooth torque-speed characteristics. Furthermore, preferences of WORMESH-II for sidewinding, lateral walking, steering, and locomotion on slope and inclined terrains will be discussed in the future.

## Appendix

The robot's movement as seen from above is depicted in Fig. 21 of translational locomotion. This motion relates to the trajectory depicted in Fig. 17.

## Supplementary Information

The online version contains supplementary material available at <https://doi.org/10.1186/s40648-023-00244-0>.

**Additional file 1: Video 1.** Translational Locomotion Experiment (Fig.16).

**Additional file 2: Video 2.** Spinning Locomotion Experiment (Fig.18).

**Additional file 3: Video 3.** Translational Locomotion Experiment (Fig.21).

## Acknowledgements

Not applicable.

## Author contributions

GR developed all locomotion gaits, programming, simulation, mathematical modelling and wrote the paper. KH contributed for hardware development. RH and SK conducted a research concept, participated in design adjustment, and drafted a paper draft assistant. All authors read and approved the final manuscript.

## Funding

This work was supported by JSPS KAKENHI Grant Number:JP16K06175.

## Availability of data and materials

Not applicable.

## Declarations

### Ethics approval and consent to participate

Not applicable.

### Consent for publication

Not applicable.

### Competing interests

The authors declare that they have no competing interests.

Received: 18 October 2022 Accepted: 30 January 2023

Published online: 28 February 2023

## References

- Zhang Z, Wang X, Wang S, Meng D, Liang B (2019) Design and modeling of a parallel-pipe-crawling pneumatic soft robot. *IEEE Access*. <https://doi.org/10.1109/ACCESS.2019.2941502>
- Omori H, Hayakawa T, Nakamura T (2008) September. Locomotion and turning patterns of a peristaltic crawling earthworm robot composed of flexible units. In 2008 IEEE/RSJ international conference on intelligent robots and systems. IEEE, p 1630-1635
- Omori H, Murakami T, Nagai H, Nakamura T, Kubota T (2012) Development of a novel bio-inspired planetary subsurface explorer: initial experimental study by prototype excavator with propulsion and excavation units. *IEEE/ASME Trans Mechatron* 18(2):459-470
- Khan MB, Chuthong T, Do CD, Thor M, Billeschou P, Larsen JC, Manoonpong P (2020) icrawl: an inchworm-inspired crawling robot. *IEEE Access*. <https://doi.org/10.1109/ACCESS.2020.3035871>
- Singh P, Ananthasuresh GK (2012) A compact and compliant external pipe-crawling robot. *IEEE Trans Rob* 29(1):251-260
- Tesch M, Lipkin K, Brown I, Hatton R, Peck A, Rembisz J, Choset H (2009) Parameterized and scripted gaits for modular snake robots. *Adv Robot* 23(9):1131-1158
- Marvi H, Gong C, Gravish N, Astley H, Travers M, Hatton RL, Mendelson JR III, Choset H, Hu DL, Goldman DI (2014) Sidewinding with minimal slip: Snake and robot ascent of sandy slopes. *Science* 346(6206):224-229
- Trebuña F, Virgala I, Pástor M, Lipták T, Miková L (2016) An inspection of pipe by snake robot. *Int J Adv Robot Syst*. <https://doi.org/10.1177/172988141666366>
- Crespi A, Ijspeert AJ (2008) Online optimization of swimming and crawling in an amphibious snake robot. *IEEE Trans Rob* 24(1):75-87
- Tesch M, Lipkin K, Brown I, Hatton R, Peck A, Rembisz J, Choset H (2009) Parameterized and scripted gaits for modular snake robots. *Adv Robot* 23(9):1131-1158
- Rasanga GVC, Hodoshima R, Kotosaka S (2021) January. The flatworm-like pedal locomotory robot WORMESH-I: locomotion based on the combination of pedal waves. In: 2021 IEEE/SICE international symposium on system integration (SII). IEEE, p 72-77
- Kano T, Watanabe Y, Ishiguro A. Sheetbot: Two-dimensional sheet-like robot as a tool for constructing universal decentralized control systems. In: 2012 IEEE international conference on robotics and automation 2012 May 14. IEEE, p 3733-3738

13. Chang MH, Chae SH, Yoo HJ, Kim SH, Kim W, Cho KJ (2019) April. Loco-sheet: Morphing inchworm robot across rough-terrain. In 2019 2nd IEEE international conference on soft robotics (RoboSoft). IEEE, p 808–813
14. Rasanga GVC, Hodoshima R, Kotosaka S (2021) August. The flatworm-like pedal locomotory robot WORMESH-II: fundamental properties of pedal wave locomotion. In: Climbing and walking robots conference. Springer, Cham, p 95–107
15. Saito M, Fukaya M, Iwasaki T (2002) Modeling, analysis, and synthesis of serpentine locomotion with a multilink robotic snake. *IEEE Control Syst Mag* 22(1):64–81
16. Li D, Wang C, Deng H, Wei Y (2020) Motion planning algorithm of a multi-joint snake-like robot based on improved serpenoid curve. *IEEE Access* 8:8346–8360
17. Wang W, Lee JY, Rodrigue H, Song SH, Chu WS, Ahn SH (2014) Locomotion of inchworm-inspired robot made of smart soft composite (SSC). *Bioinspir Biomim* 9(4):046006

### Publisher's Note

Springer Nature remains neutral with regard to jurisdictional claims in published maps and institutional affiliations.

**Submit your manuscript to a SpringerOpen<sup>®</sup> journal and benefit from:**

- ▶ Convenient online submission
- ▶ Rigorous peer review
- ▶ Open access: articles freely available online
- ▶ High visibility within the field
- ▶ Retaining the copyright to your article

---

Submit your next manuscript at ▶ [springeropen.com](https://www.springeropen.com)

---